CRYSTAL GROWTH & DESIGN

Article

pubs.acs.org/crystal

Palladium(II)−Copper(II) Assembling with Bis(2-pyridylcarbonyl)amidate and Bis(oxamate) Type Ligands

Willian X. C. Oliveira,[†] Marcos A. Ribeiro,[†] Carlos B. Pinheiro,[‡] Marinez M. da Costa,[§] Ana Paula S. Fontes,[⊥] Wallace C. Nunes,[¶] Danielle Cangussu,[∥] Miguel Julve,[#] Humberto O. Stumpf,[†] and Cynthia L. M. Pereira*[,†]

[†]Departamento de Química, Instituto de Ciências Exatas and [‡]Departamento de Física, Instituto de Ciências Exatas, Universidade Federal de Minas Gerais, Belo Horizonte, Minas Gerais 31270-901, Brazil

[§]Instituto Federal de Educação, Ciência e Tecnológica do Sudeste de Minas Gerais, IFSEMG, Juiz de Fora, Minas Gerais 36080-001, Brazil

[⊥]Departamento de Química, Instituto de Ciências Exatas, Universidade Federal de Juiz de Fora, Juiz de Fora, Minas Gerais 36036-900, Brazil

[¶]Instituto de Física, Universidade Federal Fluminense, Niterói, RJ 24210-346, Brazil

[∥]Instituto de Química, Universidade Federal de Goiás, Goiânia, Goiás 74690-900, Brazil

[#]Departament de Química Inorgànica, Instituto de Ciencia Molecular (ICMOL), Universitat de València, Paterna 46980, València, Spain

Supporting Information

ABSTRACT: Five new complexes of formula $K_4[Pd_2(mpba)_2] \cdot 4H_2O$ (**1**), $\{[K_4(H_2O)(dmso)][Pd_2(mpba)_2]\}$ (**2**), $\{[Cu(bpca)]_4[Pd_2(mpba)_2]\} \cdot 6H_2O$ (**3**), $\{[Cu(bpca)]_2[Pd(opba)]\} \cdot 1.75dmso \cdot 0.25H_2O$ (**4**), $\{[Cu(bpca)]_2[Pd(opba)]\}_n \cdot n dmso$ (**5**) [H_4mpba =1,3-phenylenebis(oxamic acid), H_4opba = 1,2-phenylenebis(oxamic acid), Hbpca = bis(2-pyridylcarbonyl)amide, and dmso = dimethyl sulfoxide] have been prepared and investigated by infrared spectroscopy, thermal analysis, single crystal X-ray diffraction, and magnetic susceptibility techniques. The structure of **2** consists of a $[Pd_2(mpba)_2]^{4-}$ anionic entity in which the palladium(II) cations are coordinated by two mpba ligands resulting in a dipalladium(II) unit that acts as a ligand toward potassium(I) cations leading to a neutral three-dimensional network. Compound **3** is a neutral hexanuclear complex where the dinuclear $[Pd_2(mpba)_2]^{4-}$ unit adopts a tetrakis(bidentate) coordination mode toward four $[Cu(bpca)]^+$ end-cap entities. This compound can be viewed as a "dimer of trimers" in which two $Cu^{II}-Pd^{II}-Cu^{II}$ trinuclear units are connected by two mpba ligands. Compounds **4** and **5** have in common the presence of a $[Pd(opba)]^{2-}$ unit, which acts as a bis(bidentate) ligand toward two $[Cu(bpca)]^+$ entities to afford neutral heterotrinuclear $Cu^{II}-Pd^{II}-Cu^{II}$ motifs that are interlinked through weak double (**4**) and single (**5**) out-of-plane copper(II) to carbonyl(bpca)-oxygen atoms leading to uniform linear (**4**) and zigzag (**5**) chains of heterobimetallic trinuclear units. The investigation of the magnetic properties of **3**−**5** in the 1.9−300 K temperature range reveals the presence of very weak antiferromagnetic interactions between the copper(II) ions. The nature and magnitude of these magnetic interactions are discussed in terms of orbital symmetry considerations.

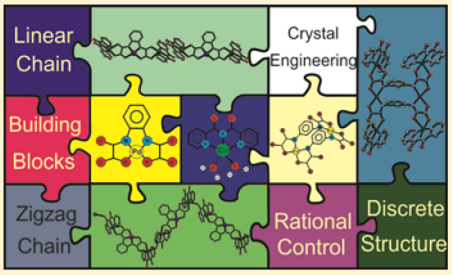

INTRODUCTION

In the last years, several building blocks have been described in the literature as examples to design molecular materials with predictable properties.[1] The major challenge that scientists face today is the control and understanding of the methods involved in the self-assembly process to obtain the desired species.[2] In this respect, and by restricting ourselves to the research fields of coordination chemistry and materials science, the metalloligand or building block approach is one of the most rewarding synthetic strategies. Indeed, the appropriate choice of the tailor-made metalloligand will determine the molecule-based architecture that can be engineered as well as the desired physical properties therein.[3−5] The richness and variety of magnetic systems based on the use of cyanide-bearing complexes[6−8] or bis- and tris(oxalate)chromate(III)[9−20] as building blocks illustrate the possibilities and broad applicability of this strategy in building new multifunctional chemical objects.

Part of our research activity was focused on the building blocks based on oxamate/oxamate-containing complexes and paid special attention to their assembling processes as well as to the main factors that can influence the reaction products (type

Received: November 28, 2014
Revised: January 30, 2015
Published: February 3, 2015

DOI: 10.1021/cg5017388
Cryst. Growth Des. 2015, 15, 1325−1335

of solvent and metal ion, temperature, concentration of reactants, pH, etc.).[21−26] Most of our efforts in this framework were devoted to the preparation of molecule-based magnets and to establish correlations between the molecular structure and the magnetic properties. In addition, we have explored the influence of molecular self-assembly and supramolecular factors envisaging the crystal engineering of oxamato-based functional materials as those which exhibit relaxation of the magnetization,[27−29] cytotoxic activity,[30] or catalytic properties.[31−33]

By keeping in mind the good coordinating properties of the oligooxamato-containing metal complexes, we have explored the possibility of preparing heterobimetallic Cu(II)−Pd(II) compounds by using the stable mononuclear $[Pd(opba)]^{2-}$ and dinuclear $[Pd_2(mpba)]^{4-}$ complexes as ligands toward the coordinatively unsaturated $[Cu(bpca)]^+$ species [H_4opba = 1,2-phenylenebis(oxamic acid), H_4mpba = 1,3-phenylenebis(oxamic acid), and Hbpca = bis(2-pyridylcarbonyl)amidate] (see Scheme 1). It deserves to be noted that this strategy allowed the preparation of polynuclear copper(II) complexes when using $[Cu(opba)]^{2-}$ instead of the palladium(II) derivative.[34]

Scheme 1. Schematic Representation of the Building Blocks $[Cu(bpca)]^+$, $[Pd(opba)]^{2-}$, and $[Pd_2(mpba)_2]^{4-}$

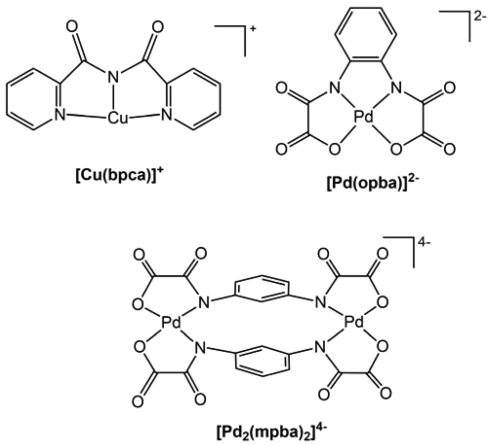

Herein, we report the preparation of the complexes $K_4[Pd_2(mpba)_2] \cdot 4H_2O$ (**1**), $\{[K_4(H_2O)(dmso)][Pd_2(mpba)_2]\}$ (**2**), $\{[Cu(bpca)]_4[Pd_2(mpba)_2]\} \cdot 6H_2O$ (**3**), $\{[Cu(bpca)]_2[Pd(opba)]\} \cdot 1.75dmso \cdot 0.25H_2O$ (**4**), $\{[Cu(bpca)]_2[Pd(opba)]\}_n \cdot n$dmso (**5**) as well as the crystal structures of **2**−**5**. The temperature dependence of magnetic susceptibility of **3**−**5** is also included in order to evaluate the magnetic interaction between the copper(II) ions through the diamagnetic oxamato-palladium(II) pathways.

EXPERIMENTAL SECTION

General. All chemicals were of analytical grade, and they were purchased from commercial sources and used as received. The palladium(II) complex $K_2[Pd(opba)] \cdot 2H_2O$ was obtained as previously reported.[35] The copper(II) complex $[Cu(bpca)(H_2O)_2]NO_3 \cdot 2H_2O$ and the proligand Et_2H_2mpba (diethyl ester derivative of H_4opba) were obtained according to literature methods.[36,37]

Synthesis of the Complexes. *$K_4[Pd_2(mpba)_2] \cdot 4H_2O$ (1).* Solid potassium hydroxide (1.056 g, 16.0 mmol) was added to a suspension of the Et_2H_2mpba proligand (1.232 g, 4.0 mmol) in water (16 mL) under continuous stirring and heating at 50 °C for 30 min. The clear solution was cooled to 40 °C, and an aqueous solution (12.0 mL) of $K_2[PdCl_4]$ (0.916 g, 2.8 mmol) was added dropwise under continuous stirring. The resulting orange solution was left to react for 120 h under continuous stirring. Then, its volume was reduced to a quarter, and the product was precipitated as a yellow solid by adding small amounts of cold methanol. The yellow solid was washed with methanol and acetone and dried under vacuum for 48 h into a desiccator. Yield: 1.208 g (69%). Anal. Calcd for $C_{20}H_{16}N_4O_{16}K_4Pd_2$ (937.56 g mol^{-1}) (**1**): C, 25.62; H, 1.72; N, 5.98. Found: C, 25.44; H, 1.95; N, 5.88%. IR (KBr, cm^{-1}): 3424 (O−H), 1671, 1646 (O=C−O$^-$ + C=O), 1596 (C=C), 1455 (O=C−O$^-$), 1314 (C−N), 834, 755 (C−H), 547 (Pd−N), 425 (Pd−O). ^{1}H NMR (D_2O, ppm): 6.82 (t, 1H, C−H_{ring}, J_{HH} = 8.0 Hz), 6.64 (d, 1H, C−H_{ring}, J_{HH} = 8.0 Hz), 6.18 (s, 1H, C−H_{ring}). ^{13}C NMR (D_2O, ppm): 171 (O=C−$O^-_{carboxylate}$), 164 (C=O_{amide}), 141 (C_{ring}), 131 (C_{ring}), 125 (C_{ring}), 124 (C_{ring}).

$\{[K_4(H_2O)(dmso)][Pd_2(mpba)_2]\}$ (2). A solid sample of **1** (0.240 g, 0.256 mmol) was dissolved in mixture of H_2O/dmso (1:1 v/v, 60.0 mL) under stirring for 10 min. The resulting yellow solution was allowed to evaporate slowly at 40 °C for 1 week. X-ray quality yellow prisms of **2** were formed during this process. They were filtered off, washed with diethyl ether, and left to dry at room temperature for 3 days. Yield: 0.246 g (65%). Anal. Calcd for $C_{22}H_{16}N_4O_{14}SK_4Pd_2$ (961.67 g mol^{-1}) (**2**): C, 27.30; H, 1.68; N, 5.83. Found: C, 27.24; H, 1.83; N, 5.76%. IR (KBr, cm^{-1}): 3424 (O−H), 1681, 1649 (O=C−O$^-$ + C=O), 1609 (C=C), 1477 (O=C−O$^-$), 1309 (C−N), 1016 (S=O), 834, 755 (C−H), 546 (Pd−N), 421 (Pd−O).

$\{[Cu(bpca)]_4[Pd_2(mpba)_2]\} \cdot 6H_2O$ (3). A solid sample of **1** (0.250 g, 0.266 mmol) was introduced into one arm of an H-shaped tube, whereas $[Cu(bpca)(H_2O)_2]NO_3 \cdot 2H_2O$ (0.250 g, 0.590 mmol) was placed into the other one. Distilled water was added dropwise to fill the H-shape, covered with parafilm, and allowed to diffuse at room temperature. Dark blue needles of **3** were grown after three months. They were filtered off, washed with water, and allowed to dry on filter paper at room temperature. Yield: 0.255 g (88%). Calcd for $C_{68}H_{52}N_{16}O_{26}Cu_4Pd_2$ (1976.26 g mol^{-1}) (**3**): C, 40.77; H, 2.45; N, 11.06; Cu, 14.10. Found: C, 41.33; H, 2.65; N, 11.34; Cu, 13.86%. IR (KBr, cm^{-1}): 3445 (O−H), 1715 (C=O_{bpca}), 1622 and 1603 (O=C−O$^-$ + C=O), 1448 (O=C−O$^-$), 1362 (C=N), 1358 (C−N), 826, 764 (C−H), 590 (Cu−O), 542 (Pd−N), 416 (Pd−O).

$\{[Cu(bpca)]_2[Pd(opba)]\} \cdot 1.75dmso \cdot 0.25H_2O$ (4). An aqueous solution (2.0 mL) of $[Cu(bpca)(H_2O)_2]NO_3 \cdot 2H_2O$ (0.020 g, 0.05 mmol) was added dropwise to a dmso solution (4.0 mL) of $K_2[Pd(opba)] \cdot 2H_2O$ (0.053 g, 0.12 mmol) under continuous stirring. The resultant blue solution was stirred vigorously for 10 min at 70 °C and then filtered off and allowed to evaporate at room temperature into an open glass crystallizer. After 3 days, dark blue needle-like crystals of **4** were grown from the mother liquor. They were collected by filtration, washed with a mixture of water and dmso (1:1 v/v), and air-dried at room temperature. Yield: 36.0 mg (66%). Anal. Calcd for $C_{37.5}H_{32}N_8O_{12}S_{1.75}Cu_2Pd$ (1076.30 g mol^{-1}) (**4**): C, 41.89; H, 2.91; N, 10.42; Cu, 11.82%. Found: C, 41.71; H, 2.45; N, 10.45; Cu, 12.55%. IR (KBr, cm^{-1}): 1716 (C=O_{bpca}), 1624 and 1602 (O=C−O$^-$ + C=O), 1456 (O=C−O$^-$), 1362 (C=N), 1356 (C−N), 1003 (S=O), 826, 764 (C−H), 587 (Cu−O), 542 (Pd−N), 419 (Pd−O).

$\{[Cu(bpca)]_2[Pd(opba)]\}_n \cdot n$dmso (5). The preparative route used for **5** is identical to that of **4**, except for the crystallization process. In the present case, the resulting solution was slowly cooled down within its silicon oil bath (~80 mL) to room temperature in a closed container. After 2 days, tabular dark green crystals of **5** were grown. They were collected and washed as done for **3**. Yield: 26.1 mg (48%). Anal. Calcd for $C_{36}H_{26}N_8O_{11}SCu_2Pd$ (1012.29 g mol^{-1}) (**5**): C, 42.72; H, 2.59; N, 11.07; Cu, 12.85. Found: C, 41.66; H, 2.48; N, 10.87; Cu, 13.01%. IR (KBr, cm^{-1}): 1715 (C=O_{bpca}), 1626 and 1600 (O=C−O$^-$ + C=O), 1456 (O=C−O$^-$), 1362 (C=N), 1356 (C−N), 1008 (S=O), 826, 767 (C−H), 586 (Cu−O), 540 (Pd−N), 421 (Pd−O).

Physical Techniques. Elemental analysis (C, H, and N) was carried out on a PerkinElmer 2400 analyzer. Atomic absorption for Cu was performed with a Hitachi Z-8200 polarized atomic absorption spectrophotometer. Infrared spectra were recorded on a PerkinElmer 882 spectrophotometer in the range of 4000−400 cm^{-1} using KBr pellets. Thermogravimetric analysis (TG/DTA) data were collected

DOI: 10.1021/cg5017388
Cryst. Growth Des. 2015, 15, 1325−1335

Table 1. Summary of the Crystal Data and Refinement Details for 2−5

compound	2	3	4	5
formula	$C_{22}H_{16}K_4N_4O_{14}Pd_2S$	$C_{68}H_{52}Cu_4N_{16}O_{26}Pd_2$	$C_{37.5}H_{32}Cu_2N_8O_{12}PdS_{1.75}$	$C_{36}H_{26}N_8O_{11}SCu_2Pd$
F_w	961.65	1963.32	1076.30	1012.19
T/K	150(2)	120(2)	150(2)	150(2)
λ/Å	1.5418	1.5418	1.5418	1.5418
cryst syst	orthorhombic	triclinic	monoclinic	orthorhombic
space group	*Pnma*	$P\bar{1}$	$P2_1/c$	*Pbca*
a/Å	22.5630 (4)	7.632(5)	10.6939(3)	22.48920(10)
b/Å	12.8816 (2)	17.925(5)	28.5378(9)	14.08580(10)
c/Å	10.2578 (2)	27.083(5)	13.6808(4)	23.87790(10)
α/deg	90	80.747(5)	90.0	90
β/deg	90	88.580(5)	101.310(3)	90
γ/deg	90	89.776(5)	90.0	90
V/Å^3	2981.40 (9)	3656(3)	4094.0(2)	7564.00(7)
Z	4	2	4	8
ρ/g cm^{-3}	2.142	1.784	1.746	1.778
μ/mm^{-1}	16.09	5.968	6.181	6.250
$F(000)$	1888	1964	2164	4040
cryst size/mm^3	0.22 × 0.05 × 0.04	0.46 × 0.07 × 0.04	0.38 × 0.15 × 0.07	0.28 × 0.19 × 0.07
reflns collected	32918	15509	50492	201442
GOF on F^2	1.10	1.08	1.126	1.022
R^a, wR^b [$I > 2\sigma(I)$]	0.026, 0.054	0.0535, 0.1420	0.0706, 0.1716	0.0400, 0.0994
R^a, wR^b (all data)	0.035, 0.058	0.0606, 0.1475	0.0890, 0.1876	0.0496, 0.1077

$^aR = \Sigma \|\|F_0| - |F_c\|| / \Sigma |F_0|$. $^bwR = \{\Sigma[w(F_0^2 - F_c^2)^2] / \Sigma[w(F_0^2)^2]\}^{1/2}$, $w = 1/[\sigma^2(F_0^2) + (aP)^2 + bP]$ (where a and b are adjustable constants, and $P = (F_0^2 + 2F_c^2)/3$.

with a Shimadzu TG/DTA 60 by using approximately 2.0 mg of the samples packed into an alumina crucible. Samples were heated at 10 °C min^{-1} from room temperature to 750 °C in a dynamic flow of dinitrogen (flow rate of 200 cm^3 min^{-1}). IR curves and TG curves are shown in the Figures S1−S10 of the Supporting Information. ^{1}H NMR spectra were obtained at room temperature with a Bruker DRX-200 Avance (200 MHz) spectrometer using deuterium oxide (D_2O) as the solvent. X-ray powder diffraction patterns for compounds **2**−**5** were obtained by using a Rigaku/Geirgeflex diffractometer at room temperature. Data were collected in the Bragg/Brentano mode (1 deg s^{-1}) by using monochromatic Cu−Kα radiation (Supporting Information, Figures S11−S14). The dc magnetic measurements were performed with a Cryogenics Sx600 SQUID magnetometer (Supporting Information, Figures S15 and S16). The diamagnetic corrections for the constituent atoms were estimated from Pascal's constants[38] as −813 × 10^{-6} (**3**), −457 × 10^{-6} (**4**), and −417 × 10^{-6} cm^3 mol^{-1} (**5**) [per four (**3**) and two (**4** and **5**) copper(II) ions]. Corrections for the temperature-independent paramagnetism [60 × 10^{-6} cm^3 mol^{-1} per Cu^{II}] and the magnetization of the sample holder were also applied.

X-ray Data Collection and Structure Refinement. X-ray diffraction data collections on single crystals of **2**−**5** were performed with an Oxford-Diffraction GEMINI-Ultra diffractometer (LabCri) by using Enhance Source Cu-Kα radiation (λ = 1.5418 Å). Measurements were performed at different temperatures as shown in Table 1. Data integration and scaling of the reflections for all compounds were performed with the *CRYSALIS* suite.[39] Final unit cell parameters were based on the fitting of all reflections positions. Analytical absorption corrections were performed using *CRYSALIS* suite,[39] and the space group identification was done with *XPREP*.[40] The structures of all compounds were solved by direct methods using the *SUPERFLIP* program.[41] For each compound, the positions of all atoms could be unambiguously assigned on consecutive difference Fourier maps. Refinements were performed using *SHELXL*[42] based on F^2 through full-matrix least-squares routine. All nonhydrogen atoms from **2**−**5** were refined with anisotropic atomic displacement parameters. All hydrogen atoms except those of the water molecules of **3** were located in difference maps and included as fixed contributions according to the riding model.[43] U_{iso}(H) = 1.5U_{eq}(O) for the water molecules, and C−H = 0.97 Å and U_{iso}(H) = 1.2U_{eq}(C) for the methylene groups. Samples of compound **3** used in the single X-ray diffraction experiments were found to be twinned. The integration of the data used in the final structure refinement was performed considering two domains rotated by 180° around the [100] axes. The refinement was performed using all overlapping and nonoverlapping reflections from both domains, and the final twin volume ratio converged to ∼0.503. There are six solvent water molecules in the structure, and some of their hydrogen atoms do not point toward any hydrogen bond acceptor in order to avoid too short van der Waals contacts. For compounds **4** and **5**, disordered solvent water and dmso molecules were observed and modeled properly. In **4**, a model of substitutional occupation between dmso and water molecules was applied. The occupancy of each molecule was determined based on the height of the peaks found in the Fourier difference maps supported by the dmso/water mass loss in the TGA experiments upon heating. For compound **5**, the Fourier difference maps indicated a disorder in the dmso molecules that was refined with split atomic positions of the molecule over two positions. Crystal, X-ray diffraction data, and refinement parameters of compounds **2**−**5** are shown in Table 1. Selected bond lengths and angles for compounds **2**−**5** are given in Tables 2−5. CCDC numbers for the structures determined in this work are 1034458 (**2**), 1034457 (**3**), 1034456 (**4**), and 1034455 (**5**).

RESULTS AND DISCUSSION

Thermal Study and IR Spectroscopy. Thermogravimetric and differential thermal analysis (TG/DTA) for **1** (Supporting Information, Figure S6) exhibits a first weight loss from room temperature until 200 °C relative to 7.8% of the total mass in an endothermic process, probably related to the loss of four water molecules (calcd. 7.7%). There are also several weight losses between 200 and 700 °C, which correspond to exothermic steps in the DTA curve, most likely due to thermal decomposition of the organic ligand. The residue at 600 °C is thermally stable, and it is composed by an equimolar mixture of PdO and K_2O (found 45.8%; calcd. 46.2%).[44]

DOI: 10.1021/cg5017388
Cryst. Growth Des. 2015, 15, 1325−1335

Table 2. Selected Bond Lengths (Å) and Angles (deg) for 2

metals environment			
Pd1–N2	1.998 (3)	N2–Pd1–N1	104.51 (11)
Pd1–N1	2.002 (3)	N2–Pd1–O1	173.49 (11)
Pd1–O1	2.024 (2)	N1–Pd1–O1	81.87 (10)
Pd1–O4	2.028 (2)	N2–Pd1–O4	81.57 (10)
K1–O3^{ii}	2.802 (2)	N1–Pd1–O4	173.90 (10)
K1–O3^{i}	2.802 (2)	O1–Pd1–O4	92.03 (9)
K1–O7	2.829 (4)	O3^{ii}–K1–O3^{i}	119.82 (11)
K1–O1	2.865 (2)	O3^{ii}–K1–O7	70.29 (7)
K1–O1^{iii}	2.865 (2)	O3^{i}–K1–O7	70.29 (7)
K1–O2^{iii}	2.884 (3)	O3^{ii}–K1–O1	152.30 (8)
K1–O2	2.884 (3)	O3^{i}–K1–O1	73.91 (7)
K2–O6^{iv}	2.660 (3)	O7–K1–O1	95.36 (8)
K2–O3	2.692 (3)	O3^{ii}–K1–O1^{iii}	73.91 (7)
K2–O2	2.771 (3)	O3^{i}–K1–O1^{iii}	152.30 (8)
K2–O5^{iv}	2.887 (3)	O7–K1–O1^{iii}	95.36 (8)
K2–O8w	2.9933 (11)	O1–K1–O1^{iii}	84.41 (10)
K2–O4^{v}	3.084 (3)	O3^{ii}–K1–O2^{iii}	80.59 (8)
K2–O1^{v}	3.300 (3)	O3^{i}–K1–O2^{iii}	152.32 (8)
K3–O4^{iii}	2.770 (2)	O7–K1–O2^{iii}	137.23 (7)
K3–O6^{ix}	2.800 (2)	O1–K1–O2^{iii}	96.54 (8)
K3–O6^{vii}	2.800 (2)	O1^{iii}–K1–O2^{iii}	45.53 (7)
K3–O5^{iii}	2.866 (3)	O3^{ii}–K1–O2	152.32 (8)
K3–C9^{vii}	3.126 (5)	O3^{i}–K1–O2	80.59 (8)
K3–C7^{iii}	3.177 (4)	O7–K1–O2	137.23 (7)
K3–C8^{ix}	3.436 (3)	O1–K1–O2	45.52 (7)
K3–C8^{vii}	3.436 (3)	O1^{iii}–K1–O2	96.54 (8)
		O2^{iii}–K1–O2	74.63 (11)
		O6^{iv}–K2–O2	108.49 (8)
		O3–K2–O2	60.84 (7)
		O6^{iv}–K2–O5^{iv}	59.76 (7)
		O3–K2–O5^{iv}	171.82 (8)
		O2–K2–O5^{iv}	111.58 (8)
		O6^{iv}–K2–O8w	117.44 (11)
		O3–K2–O8w	111.53 (11)
		O2–K2–O8w	66.24 (10)
		O5^{iv}–K2–O8w	65.50 (10)
		O6^{iv}–K2–O4^{v}	73.19 (7)
		O3–K2–O4^{v}	114.32 (7)
		O2–K2–O4^{v}	175.15 (8)
		O5^{iv}–K2–O4^{v}	73.24 (7)
		O8w–K2–O4^{v}	117.32 (10)
		O6^{iv}–K2–O1^{v}	119.58 (7)
		O3–K2–O1^{v}	68.45 (7)
		O2–K2–O1^{v}	121.89 (7)
		O5^{iv}–K2–O1^{v}	119.67 (7)
		O8w–K2–O1^{v}	112.19 (10)
		O4^{v}–K2–O1^{v}	54.21 (6)
		K2–O8w–K2^{iii}	168.84 (17)
		O4^{iii}–K3–O6^{ix}	76.31 (7)
		O4–K3–O6^{ix}	162.90 (8)
		O7–K3–O6^{vii}	78.86 (7)
		O4^{iii}–K3–O6^{vii}	162.90 (8)
		O4–K3–O6^{vii}	76.31 (7)
		O6^{ix}–K3–O6^{vii}	119.78 (10)
		O7–K3–O5	141.34 (6)
		O4^{iii}–K3–O5	97.35 (8)
		O4–K3–O5	46.57 (7)
		O6^{ix}–K3–O5	139.06 (8)
		O6^{vii}–K3–O5	74.46 (7)
		O7–K3–O5^{iii}	141.34 (6)
		O4^{iii}–K3–O5^{iii}	46.57 (7)
		O4–K3–O5^{iii}	97.35 (8)
		O6^{ix}–K3–O5^{iii}	74.46 (7)
		O6^{vii}–K3–O5^{iii}	139.06 (8)
		O5–K3–O5^{iii}	72.53 (10)
		K3–O7–K1	112.53 (15)

hydrogen bonds[a,b]				
D–H···A	D–H/Å	H···A/Å	*D*···A/Å	D–H···A/deg
O8–H10···O5^{iv}	0.89 (2)	2.49 (2)	3.182 (4)	136 (1)
O8–H11···O2	0.89 (2)	2.48 (2)	3.155 (4)	133 (1)

[a]D = donor, and A = acceptor. [b]Symmetry code: (iv) = 1/2 + *x*, *y*, 1/2 − *z*.

TGA/DTA curves for **2** (Supporting Information, Figure S7) exhibit the first weight loss between 80 and 150 °C, which corresponds to the loss of one water molecule (found 2.2%; calcd. 1.8%). The compound is thermally stable between 150 and 300 °C when it starts to undergo successive mass losses in exothermic steps associated with the evaporation of the dmso molecule concomitantly with thermal decomposition of the mpba ligand. The heating process ends at 700 °C, and an amount of residue most likely being PdO was obtained (found 51.1%; calcd. 51.7%).

TGA/DTA curves for **3** (Supporting Information, Figure S3) exhibit one first weight loss between room temperature and 150 °C, which corresponds to 5.31% of the initial mass and is associated with an endothermic process in the DTA curve. This mass loss is tentatively attributed to the evaporation of six water molecules (calcd. 5.46%). Three weight losses in the temperature range of 150–600 °C are associated with the thermal degradation of the bpca and mpba ligands. At 600 °C, the residue (36.43% of the initial mass) probably contains an equimolar mixture of PdO and Cu_2O plus some amount of carbonized material.

The TGA curve of **4** (Supporting Information, Figure S4) depicted a first weight loss between room temperature and 235 °C in an endothermic process associated probably to the loss of 1.75 dimethyl sulfoxide and 0.25 water molecules (found 13.13%; calcd. 13.10%). In a second step, opba and bpca ligands decompose between 245 and 560 °C, and above this temperature, a residue is obtained, probably associated with the mixture of PdO and Cu_2O in the solid state (found 25.44%; calcd. 25.81%).

The TGA curve for **5** (Supporting Information, Figure S5) shows a continuous loss of mass from room temperature until the end of the analysis. Between 25 and 300 °C, 7.65% of the initial mass is lost in an endothermic process, which can be associated with the removal of one molecule of dmso (calcd. 7.71%) as expected. Above 300 °C, an exothermic process takes place, which is related to the thermal decomposition of the opba and bpca ligands.

The IR spectra of all compounds are in agreement with the molecular formulas determined by elemental analysis and single crystal X-ray diffraction data. The IR spectra of **1** and **2** (Supporting Information, Figures S6 and S7) are very similar, except for the presence of an intense and large peak at 1016

DOI: 10.1021/cg5017388
Cryst. Growth Des. 2015, 15, 1325–1335

cm^{-1} in the spectrum of **2** that does not appear in **1**, which is attributed to the stretching vibration of the S=O bond of the dmso molecule of crystallization. The analysis of the IR spectrum of **2** in more details reveals that the lack of the O–$C_{aliphatic}$ ester stretch vibrations at 1288 and 1267 cm^{-1} and the presence of peaks at about 1455 cm^{-1} (carboxylate symmetric stretching) support the complete hydrolysis of the ester group. The shifts of the carbonyl bands from 1725 and 1700 cm^{-1} to 1671 and 1645 cm^{-1} are due to the effect of a heavy atom bonded to both amide and carboxylate groups, a feature that becomes an indication of coordination. The absence of N–H stretching vibrations suggests that the amidate nitrogen may be involved in the chelation. Finally, the presence of bands at 547 and 425 cm^{-1} is tentatively assigned to the stretching vibrations of the Pd–N and Pd–O bonds, respectively.[30]

The infrared spectra of **2** and **3** (Supporting Information, Figures S7 and S8) are quite similar since they have the same $[Pd_2(mpba)_2]^{4-}$ building block. The main differences among them can be associated with the occurrence of the S=O stretching vibration at 1016 cm^{-1} due to the dmso molecules in **2** and to the presence of a strong peak at 1715 cm^{-1} (C=O_{imide} stretching), which unambiguously supports the existence of the $[Cu(bpca)]^+$ fragment in **3**.[34]

As far as the infrared spectra of **4** and **5** are concerned (Supporting Information, Figures S9 and S10), they are also very similar because of the presence of the same $[Pd(opba)]^{2-}$ and $[Cu(bpca)]^+$ fragments, the C=O_{imide} stretching vibrations are centered at 1715 (**4**) and 1716 cm^{-1} (**5**).

Description of the Structures. All our attempts to get single crystals of **1** were unsuccessful. Given that the knowledge of the precursor is crucial in order to use it as a ligand in the programmed stepwise route envisaging tailor-made polynuclear species, we focused on the dmso as solvent and in so doing, X-ray quality crystals of **2** were successfully grown.

{[$K_4(H_2O)$(dmso)][Pd_2(mpba)$_2$]} (**2**). The crystal structure of **2** consists of dipalladium(II) $[Pd_2(mpba)_2]^{4-}$ units, potassium-(I) cations (Figure 1a), and coordinated dmso and water molecules. The $[Pd_2(mpba)_2]^{4-}$ tetra-anionic unit is a metallamacrocycle of the [3,3]metallacyclophane type connected by two N–Pd–N bonds. Each palladium(II) ion is four-coordinate in a square planar geometry with values of the bond lengths [Pd–N = 1.998 and 2.002 Å; Pd–O = 2.024 and 2.028 Å] and bond angles subtended by the oxamato fragments at the palladium atom [81.87 and 81.57° for N1–Pd1–O1 and N2–Pd1–O4, respectively] that agree with those observed in other structures of bis(oxamato)palladate(II) complexes [values of Pd–N, Pd–O, and N–Pd–O in the ranges 1.99–2.04 Å, 1.97–2.04 Å, and 81.2–82.7°, respectively].[30−33,35] The two aromatic rings of the mpba ligand within each dipalladium(II) core are quasi parallel and face each other by means of π-stacking interactions. The average distance and the angle between the ring planes are 3.36(5) Å and 11.66(22)°, respectively. The intramolecular distance involving two palladium(II) atoms is 6.8241(5) Å, whereas the angle between the square planes at the palladium(II) ions is 105.57(6)°. These values compare well with those found in the related dicopper(II) complex $\{[Na_4(H_2O)_7][Cu_2(mpba)_2(H_2O)]\} \cdot 2H_2O$ [6.822(3) Å and 122.2(2)°] whose structure and magnetic study were reported earlier.[37]

The packing of **2** (Figure 1b) shows the supramolecular 3D network constituted by $[Pd_2(mpba)_2]^{4-}$ anions and K^+ as counterions situated between the anionic units and interacting with all oxygen atoms. The view of this supramolecular polymer

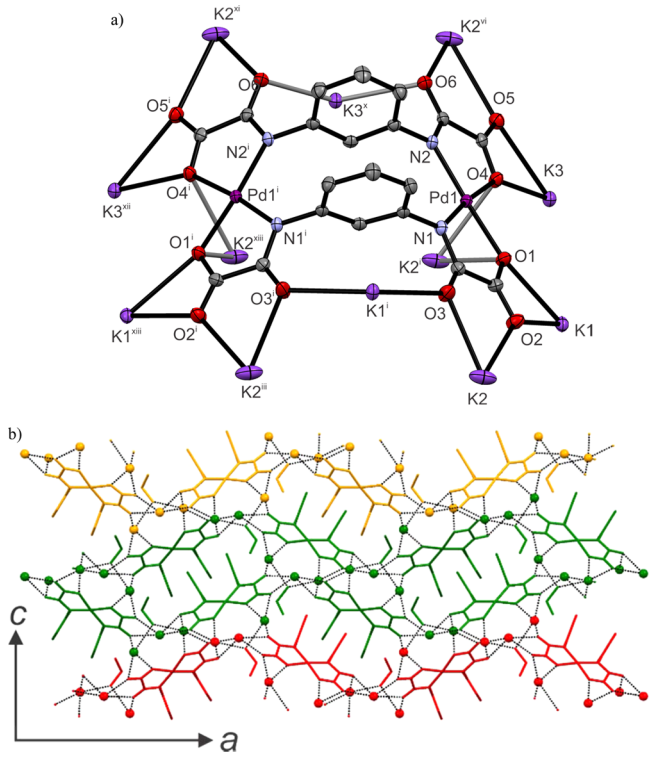

Figure 1. (a) Perspective drawing of the $[Pd_2(mpba)_2]^{4-}$ unit of **2** illustrating its coordination modes toward the potassium(I) cations. The atom numbering is limited to the metal centers and to nitrogen and oxygen atoms of the oxamate groups. Thermal ellipsoids are drawn at 50% probability level. The dmso and water molecules as well as the hydrogen atoms were omitted for sake of clarity. [Symmetry codes: (*i*) = *x*, −1/2 − *y*, *z*; (*iii*) = *x*, 1/2 − *y*, *z*; (*vi*) = 1/2 + *x*, *y*, −1/2 + *z*; (*x*) = 1 − *x*, −1/2 + *y*, 1 − *z*; (*xi*) = 1/2 + *x*, −1/2 − *y*, 1/2 − *z*; (*xii*) = *x*, 1 − *y*, *z*; (*xiii*) = 1/2 − *x*, −1/2 + *y*, 1/2 + *z*]. (b) View of the crystal packing of **2** down the crystallographic *b*-axis showing the supramolecular 3D network. Different colors were used to make the view of the structural pattern easier. Black dotted lines represent the potassium bonds connecting the waving layers and the $[Pd_2(mpba)_2]^{4-}$ cores.

along the crystallographic *b*-axis shows a wave-like packing in *a* × *c* plane with a value of 10.7233(3) Å for the distance between the $[Pd_2(mpba)_2]^{4-}$ cores. Three crystallographically independent potassium(I) cations (K1, K2, and K3) occur in **2**, and their surroundings are shown in Figure 2. They are eight- (K1) and seven-coordinate (K2 and K3) with six oxamate-oxygen atoms (K1, K2, and K3), shared water molecules [K2 and $K2^{iii}$ symmetry code: (iii) = *x*, 1/2 − *y*, *z*] and shared dmso-oxygen atoms (K2 and K3), and a cation-π type interaction (K1) with the phenyl ring defined by the C3C4C5C6C5^{i}C4^i set of atoms [symmetry code: (i) = *x*, −1/2 − *y*, *z*],[45,46] which results in distorted square antiprism (K1) and monocapped octahedral (K2 and K3) environments. The distance between the K1 and the ring centroid of the aromatic ring is 3.14(4) Å, and the value of the angle between the normal to the aromatic ring and the ring-centroid to K1 is 2.0(2)°. The main difference between the 3D supramolecular array of **2** and that of the parent dicopper(II) derivative already described, $\{[Na_4(H_2O)_7][Cu_2(mpba)_2(H_2O)]\} \cdot 2H_2O$,[20] may be explained by the nature of the solvent (water:dmso vs water) and univalent alkaline cation [potassium(I) against sodium(I)] used in their preparations.

DOI: 10.1021/cg5017388
Cryst. Growth Des. 2015, 15, 1325−1335

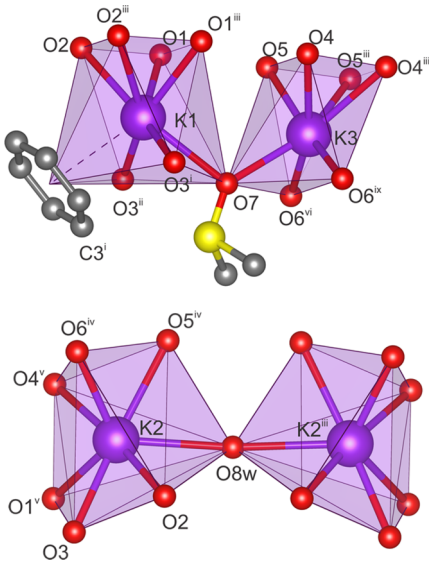

Figure 2. View of the surroundings of the three crystallographically independent potassium(I) cations in **2**. [Symmetry codes: (i) = 1/2 − *x*, −*y*, 1/2 + *z*; (ii) = 1/2 − *x*, 1/2 + *y*, 1/2 + *z*; (iii) = *x*, 1/2 − *y*, *z*; (iv) = −1/2 + *x*, *y*, 1/2 − *z*; (v) = 1/2 − *x*, −*y*, −1/2 + *z*; (vi) = 1/2 + *x*, *y*, 1/2 − *z*; (vii) = 1 − *x*, −*y*, 1 − *z*].

Besides the coordination to potassium atoms, the dmso and water of crystallization also act as filling space molecules. In this structure, the water molecules prefer to maximize the distance between potassium(I) in detriment to form hydrogen bonds. The hydrogen bonds in **2** have a D−H···A angle far from linearity (see bottom of Table 2), a feature that supports a low directionality in this type of interaction, which is considered to be more electrostatic than covalent.[47]

{[Cu(bpca)]$_4$[Pd$_2$(mpba)$_2$]} · 6H$_2$O (**3**). The crystal structure of compound **3** consists of neutral hexanuclear {[Cu(bpca)]$_4$[Pd$_2$(mpba)$_2$]} units and crystallization water molecules (Figure 3a). Each hexanuclear entity is formed by four $[Cu(bpca)]^+$ cations and one dinuclear $[Pd_2(mpba)_2]^{4-}$ anion. The aromatic rings of the two mpba ligands almost face each other [values of 2.86(8)° and 3.265(10) Å for the dihedral angle between the mean planes and the interplanar distance, respectively]. The palladium−palladium separation across the cyclophane moiety is 7.0226(16) Å, a value that is almost 20% longer than that found for the Cu···Cu in the [*N*,*N*′-1,3-phenylenebis(oxamato)]dicopper(II) complex of formula {[Na$_4$(H$_2$O)$_7$][Cu$_2$(mpba)$_2$(H$_2$O)]} · 2H$_2$O.[20] The two crystallographically independent palladium(II) ions [Pd1 and Pd2] are four-coordinate in a somewhat distorted square planar geometry as in **2**. The values of Pd−N and Pd−O bond lengths cover the ranges of 1.998(8)−2.004(8) and 2.026(6)−2.040(6) Å, respectively, whereas those of the N−Pd−O bond angles vary in the narrow range of 81.6(3)−82.0(3)° (see Table 3). The four crystallographically independent copper(II) ions (Cu1, Cu2, Cu3, and Cu4) are five-coordinate in somewhat distorted square pyramidal surroundings, the values of the trigonality parameter (τ) being 0.14 (Cu1 and Cu2), 0.25 (Cu3), and 0.17 (Cu4) [τ = 0 and 1 for ideal square pyramid and trigonal bipyramid, respectively].[48] The basal positions at the copper(II) ions are occupied by the three nitrogen atoms from the bpca ligand (Cu1, Cu2, Cu3, and Cu4) and either one carboxylate(oxamate)-oxygen (Cu1 and Cu3) or an amidate(oxamate)-oxygen (Cu2 and Cu4). The apical sites are filled by

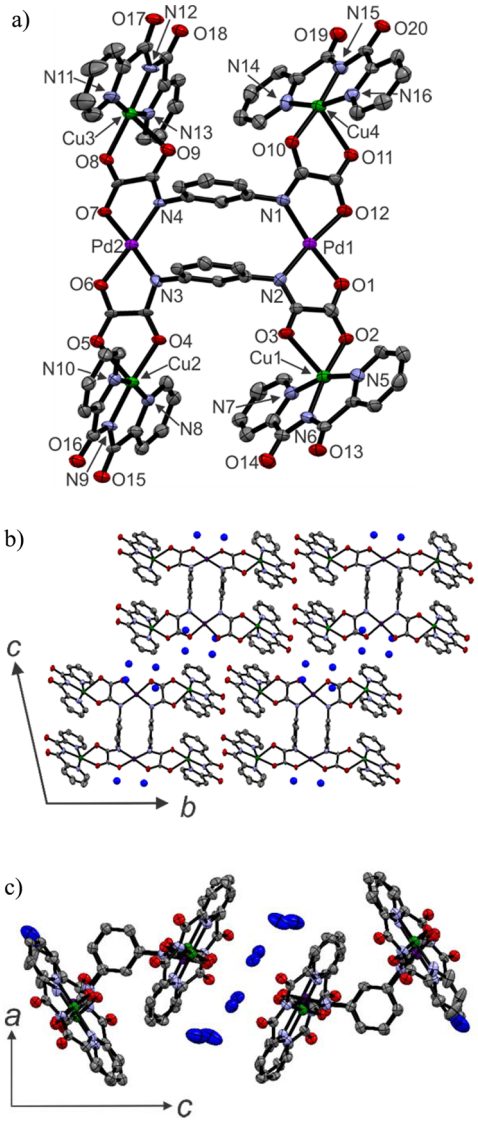

Figure 3. (a) Perspective of view of **3** together with the numbering scheme for the noncarbon atoms. Thermal ellipsoids are drawn at the 50% probability level. Solvent molecules and hydrogen atoms were omitted for sake of clarity. (b, c) Views of the crystal packing of **3** along the crystallographic *b*- and *c*-axes. The water oxygen ellipsoids were drawn in dark blue for clarity.

either one amidate(oxamate)-oxygen (Cu1 and Cu3) or a carboxylate(oxamate)-oxygen (Cu2 and Cu4). The Cu−N$_{bpca}$ bond distances vary in the ranges of 1.932(8)−1.999(9) (at Cu1), 1.915(7)−2.010(9) (at Cu2), 1.947(7)−2.007(6) (at Cu3), and 1.924(8)−2.008(8) Å (at Cu4), with the inner Cu−N bond length being shorter than the outer ones. These values are in agreement with those reported previously for several [bis(2-arylcarbonyl)amidate]copper(II) complexes.[34,46,49−56] The distance between palladium(II) and copper(II) through the oxamato bridge varies from 5.397(2)−5.467(2) Å and between two copper(II) ions are 10.752(4) (Cu1···Cu4), 10.888(4) (Cu2···Cu3), 13.505(4) (Cu1···Cu3), 13.013(3) (Cu2···Cu4), 7.644(3) (Cu1···Cu2), and 7.748(3) Å (Cu3···Cu4). It is worth nothing that the $[Cu(bpca)]^+$ units from the linear Cu−Pd−Cu fragments are antiparallel and also that the mean planes of the bpca ligands on the same side of each mpba ligand form a dihedral angle of 51.6(4)°. The presence of four $[Cu(bpca)]^+$ units in the complex rearranges the

DOI: 10.1021/cg5017388
Cryst. Growth Des. 2015, 15, 1325−1335

Table 3. Selected Bond Lengths and Angles for 3

Pd2–N3	1.998 (7)	N3–Pd2–O6	174.2 (3)
Pd2–N2	2.004 (8)	N2–Pd2–O6	82.0 (3)
Pd2–O7	2.029 (6)	N3–Pd2–O7	81.8 (3)
Pd2–O6	2.035 (6)	O7–Pd2–O6	92.7 (2)
Pd1–N1	1.998 (8)	N1–Pd1–N4	104.3 (3)
Pd1–N4	2.002 (7)	N1–Pd1–O1	81.7 (3)
Pd1–O1	2.026 (6)	N4–Pd1–O1	173.4 (3)
Pd1–O12	2.040 (6)	N1–Pd1–O12	173.6 (3)
Cu1–N6	1.932 (8)	N4–Pd1–O12	81.6 (3)
Cu1–O2	1.983 (6)	O1–Pd1–O12	92.2 (3)
Cu1–N7	1.999 (9)	N6–Cu1–O2	171.7 (3)
Cu1–N5	1.999 (8)	N6–Cu1–N7	82.8 (3)
Cu1–O3	2.275 (6)	O2–Cu1–N7	98.6 (3)
Cu2–N9	1.915 (7)	N6–Cu1–N5	82.5 (3)
Cu2–O4	1.972 (6)	O2–Cu1–N5	94.8 (3)
Cu2–N8	2.005 (9)	N7–Cu1–N5	163.1 (3)
Cu2–N10	2.010 (9)	N6–Cu1–O3	109.0 (3)
Cu2–O5	2.356 (6)	O2–Cu1–O3	79.3 (2)
Cu3–N12	1.947 (7)	N7–Cu1–O3	87.0 (3)
Cu3–N11	2.001 (10)	N5–Cu1–O3	105.7 (3)
Cu3–N13	2.005 (9)	N9–Cu2–O4	170.9 (3)
Cu3–O8	2.007 (6)	N9–Cu2–N8	82.1 (3)
Cu3–O9	2.361 (7)	O4–Cu2–N8	101.3 (3)
Cu4–N15	1.924 (8)	N9–Cu2–N10	82.6 (3)
Cu4–O10	1.946 (6)	O4–Cu2–N10	92.8 (3)
Cu4–N14	2.002 (8)	N8–Cu2–N10	162.7 (3)
Cu4–N16	2.008 (8)	N9–Cu2–O5	111.1 (3)
Cu4–O11	2.346 (6)	O4–Cu2–O5	77.4 (2)
		N8–Cu2–O5	90.5 (3)
		N10–Cu2–O5	102.4 (3)
		N12–Cu3–N11	81.2 (4)
		N12–Cu3–N13	83.0 (4)
		N11–Cu3–N13	162.0 (3)
		N12–Cu3–O8	177.2 (3)
		N11–Cu3–O8	98.8 (3)
		N13–Cu3–O8	96.7 (3)
		N12–Cu3–O9	106.2 (3)
		N11–Cu3–O9	88.9 (3)
		N13–Cu3–O9	103.8 (3)
		O8–Cu3–O9	76.5 (2)
		N15–Cu4–O10	173.6 (3)
		N15–Cu4–N14	82.6 (3)
		O10–Cu4–N14	93.8 (3)
		N15–Cu4–N16	82.7 (3)
		O10–Cu4–N16	100.2 (3)
		N14–Cu4–N16	163.4 (3)
		N15–Cu4–O11	107.4 (3)
		O10–Cu4–O11	78.4 (2)
		N14–Cu4–O11	102.3 (3)
		N16–Cu4–O11	89.3 (3)

$[Pd_2(mpba)_2]^{4-}$ core: the aromatic rings turn more eclipsed in **3** than in **2**, and the angle between the mpba aromatic rings decreases from 11.66(22) (**3**) to 2.86(8)° (**2**), the distance between the centroids being reduced from 3.36(5) (**3**) to 3.26(1) Å (**2**). Likewise, the palladium(II) ions become slightly out from the plane of their four coordinated atoms [0.014(2) Å for **2** and 0.042(4) (Pd1) and 0.040(4) Å (Pd2) for **3**].

Views of the crystal packing of **3** are shown in Figure 3, panels b and c. It can be seen therein how the disordered water molecules are placed between $[Cu(bpca)]^+$ units. The shortest intermolecular metal–metal distances are 7.989(3), 7.279(2), and 7.457(2) for Cu1···Cu1^i, Pd1···Pd1^i, and Pd1···Cu1^i, respectively [symmetry code: (i) = $1-x$, $1-y$, $1-z$].

{[Cu(bpca)]$_2$[Pd(opba)]} · 1.75dmso · 0.25H$_2$O (**4**). The structure of the asymmetric unit of **4** is made up of discrete {[Cu(bpca)]$_2$[Pd(opba)]} heterobimetallic units and uncoordinated water (O14) and dmso [S1 and S2] solvent molecules (Figure 4; Figure S17 of the Supporting Information). The

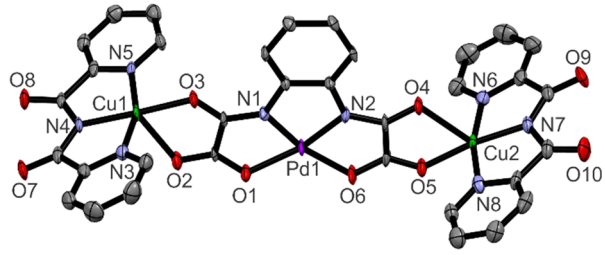

Figure 4. Perspective of view of the neutral {[Cu(bpca)]$_2$[Pd(opba)]} unit of **4** with labeling of the noncarbon atoms. Thermal ellipsoids are represented at 50% of probability level. The solvent molecules and the hydrogen atoms were omitted for clarity.

solvent molecules fill the voids between the neutral complexes. The inner $[Pd(opba)]^{2-}$ unit acts as a bis-bidentate ligand toward two peripheral $[Cu(bpca)]^+$ fragments to form a neutral Cu^{II}–Pd^{II}–Cu^{II} trinuclear complex.

Each palladium(II) ion is in a slightly distorted square planar surrounding being coordinated by two deprotonated amide-nitrogen and two carboxylate-oxygen atoms from the opba ligand. The bond distances and angles around the palladium atom in **4** (see Table 4) are very close to those observed in the mononuclear complexes $(PPh_4)_2[Pd(opba)]$[35] (PPh_4^+ = tetraphenylphosphonium) and $[Pd(NH_3)_4][Pd(opba)]$[30] and

Table 4. Selected Bond Lengths and Angles for 4

Pd1–N1	1.918 (5)	N1–Pd1–N2	83.9 (2)
Pd1–N2	1.931 (5)	N1–Pd1–O1	83.2 (2)
Pd1–O1	2.061 (4)	N2–Pd1–O1	167.1 (2)
Pd1–O6	2.076 (5)	N1–Pd1–O6	166.8 (2)
Cu1–N4	1.929 (5)	N2–Pd1–O6	83.0 (2)
Cu1–O3	1.947 (4)	O1–Pd1–O6	109.82 (18)
Cu1–N5	2.005 (6)	N4–Cu1–O3	177.2 (2)
Cu1–N3	2.014 (6)	N4–Cu1–N5	82.0 (2)
Cu1–O2	2.342 (5)	O3–Cu1–N5	98.1 (2)
Cu2–N7	1.917 (5)	N4–Cu1–N3	82.5 (2)
Cu2–O5	1.977 (5)	O3–Cu1–N3	96.9 (2)
Cu2–N8	1.978 (6)	N5–Cu1–N3	161.7 (2)
Cu2–N6	1.992 (6)	N4–Cu1–O2	104.66 (19)
Cu2–O4	2.346 (4)	O3–Cu1–O2	78.10 (18)
		N5–Cu1–O2	95.89 (19)
		N3–Cu1–O2	97.5 (2)
		N7–Cu2–O5	170.4 (2)
		N7–Cu2–N8	83.3 (2)
		O5–Cu2–N8	96.9 (2)
		N7–Cu2–N6	82.4 (2)
		O5–Cu2–N6	96.8 (2)
		N8–Cu2–N6	165.5 (2)
		N7–Cu2–O4	112.0 (2)
		O5–Cu2–O4	77.59 (17)
		N8–Cu2–O4	92.8 (2)
		N6–Cu2–O4	94.9 (2)

DOI: 10.1021/cg5017388
Cryst. Growth Des. 2015, 15, 1325–1335

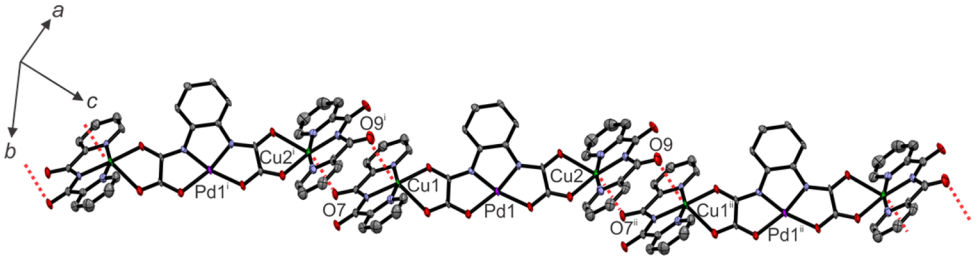

Figure 5. A view of the interconnection of the neutral heterotrinuclear units in **4** through double out-of-plane Cu···O_{bpca} interactions (dashed red lines) leading to a chain growing along the crystallographic [3/2 3/2 1] direction.

in the chain compound $\{[Co(H_2O)_2Pd(opba)] \cdot dmso\}_n$.[35] The outer bond angle at the palladium(II) ion [O1−Pd1−O6 = 109.82(16)°] is larger than the inner ones [values in the range of 83.0(2)−83.9(2)°] as expected for a planar complex with a fused 5−5−5 ring chelate system. In comparison with the structure of the trinuclear complex $\{[Cu(bpca)]_2[Cu(opba)(H_2O)]\}$ recently described,[34] the two copper(II) ions from the peripheral $[Cu(bpca)]^+$ units (Cu1 and Cu2) are crystallographically independent, being five-coordinate in distorted square pyramidal surroundings with τ values of 0.26 (Cu1) and 0.08 (Cu2). The bpca-nitrogen atoms [N3, N4, and N5 (at Cu1) and N6, N7, and N8 (at Cu2)] and the amide(oxamate)-oxygen O3 (at Cu1)/carboxylate(oxamate)-oxygen O5 (at Cu2) atoms from the opba ligand build the basal plane, whereas the apical position is occupied by the carboxylate(oxamate)-oxygen O2 (at Cu1)/amide(oxamate)-oxygen O4 (at Cu2). The Cu−N_{bpca} bond lengths present values in the ranges of 1.929(5)−2.014(6) Å around Cu1 and 1.917(5)−1.992(6) Å around Cu2. These values agree with those observed in **3** and in other bpca-containing copper(II) complexes.[34,36,49−56] The values of the Pd···Cu separation through the oxamato bridges are 5.401(1) [Pd1···Cu1] and 5.438(1) Å [Pd1···Cu2], and that for the Cu1···Cu2 distance is 10.479(1) Å. The heterometallic trinuclear units are interconnected through double out-of-plane copper(II) to carbonyl(bpca)-oxygen weak interactions [3.095(6) and 2.877(6) Å for Cu1···O9^i and Cu2^i···O7, respectively] leading to a chain of trinuclear neutral motifs with an intertrimer copper−copper separation of 5.180(1) Å [Cu1···Cu2^i; symmetry code: (i) = −1 + *x*, *y*, −1 + *z*] (see Figure 5).

*$\{[Cu(bpca)]_2[Pd(opba)]\}_n \cdot ndmso$ (**5**).* The neutral trinuclear $\{[Cu(bpca)]_2[Pd(opba)]\}$ motif occurring in **5** (see Figure 6) is similar to that of **4**, but only one dmso molecule of crystallization is present in **5**. Apart from the different number of crystallization solvent molecules between **4** and **5**, the orientation of the end-cap $[Cu(bpca)]^+$ fragments versus the inner $[Pd(opba)]^{2-}$ unit in these structures also differs somewhat. In fact, the mean planes of the bpca-containing copper(II) motifs in **4** and **5** are almost parallel between them [dihedral angle between the mean basal planes of Cu1 and Cu2 of 10.94(14) (**4**) and 10.37(12)° (**5**)], but they are closer to the orthogonality with the $[Pd(opba)]^{2-}$ unit in **4** [dihedral angles of 85.34(16) (Cu1/Pd1) and 87.03(16)° (Pd1/Cu2) in **4** versus 78.71(9) (Cu1/Pd1) and 77.58(9)° (Cu2/Pd1) in **5**].

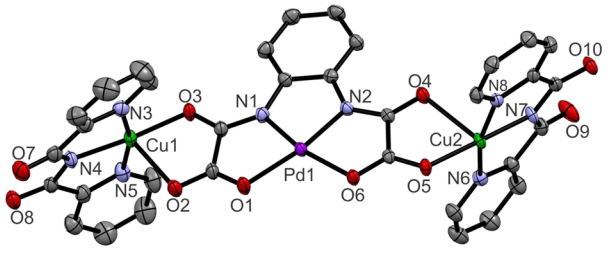

Figure 6. Perspective view of the neutral heterobimetallic trinuclear unit of **5** with the atom numbering scheme related to the noncarbon atoms. Thermal ellipsoids are represented at the 50% probability level. Solvent molecules and hydrogen atoms are omitted for clarity.

The palladium(II) ion in **5** is four-coordinate in a square planar geometry with values of bond distances and angles very similar to those reported for **4**. Again, the constrained fused 5−5−5 ring chelate at the Pd^{II} ion accounts for the opening of the outer O1−Pd1−O6 angle [109.51(11)°] with respect to the inner ones [values in the range of 82.65(12)−84.77(13)°] (see Table 5). Two crystallographically independent copper(II) ions (Cu1 and Cu2) occur in **5**, and they are five- (Cu1) and six-coordinate (Cu2) in distorted square pyramidal (τ = 0.18) and elongated octahedral surroundings, respectively. Three bpca-nitrogen atoms [N3, N4, and N5 (at Cu1) and N6, N7, and N8 (at Cu2)] and either an amidate-oxygen [O3 (at Cu1)] or a carboxylate-oxygen [O5 (at Cu2)] of the opba ligand occupy the basal (Cu1)/equatorial (Cu2) positions, whereas the apical (Cu1) and axial (Cu2) sites are filled by another carboxylate-oxygen atom [O2 at Cu1]) and an oxamate-oxygen and carbonyl(bpca)-oxygen atoms [O4 and O8^{ii} (at Cu2)]. The values of the Cu−N_{bpca} bond lengths vary in the ranges of 1.929(3)−2.010(4) (around Cu1) and 1.928(3)−2.015(3) Å (around Cu2), and they are very close to those observed in **4**. The apical (at Cu1)/axial (at Cu2) copper(II) to oxygen distances are longer [2.268(3), 2.367(3), and 2.622(3) Å for Cu1−O2, Cu2−O4, and Cu2−O8^{ii}, respectively] than the basal [Cu1−O3 = 1.975(3) Å]/equatorial [Cu2−O5 = 1.977(3) Å] ones.

In fact, the heterobimetallic units in **5** are interlinked by the weak axial Cu2−O_{bpca} interaction to afford a zigzag chain of neutral Cu1−Pd1−Cu2 trinuclear motifs running parallel to the crystallographic *c*-axis (see Figure 7). The value of the dihedral angle between the mean planes of adjacent trinuclear units in **5** is 93.5(5)°, and those of the intrachain copper−copper and palladium−copper separations are 5.6934(7) Å [Cu1···Cu2^i], 10.6917(7) Å [Cu1···Cu2], 5.3585(6) Å [Pd1···Cu1], and 5.4014(6) Å [Pd1···Cu2]. It deserves to be noted that the interconnection of the neutral trinuclear units though weak axial copper(II) to carbonyl(bpca)-oxygen interactions led to uniform linear (**4**) and zigzag (**5**) chains of Cu^{II}−Pd^{II}−Cu^{II} trinuclear entities.

The measured powder X-ray diffraction patterns for compounds **2**−**5** as well as the simulated ones obtained from the single crystal structure are shown in the Supporting Information (Figures S11−S14). The agreement between these

DOI: 10.1021/cg5017388
Cryst. Growth Des. 2015, 15, 1325−1335

Table 5. Selected Bond Lengths and Angles for 5[a]

Pd1–N2	1.931 (3)	N2–Pd1–N1	84.77 (13)
Pd1–N1	1.937 (3)	N2–Pd1–O1	167.75 (12)
Pd1–O1	2.062 (3)	N1–Pd1–O1	83.03 (12)
Pd1–O6	2.075 (3)	N2–Pd1–O6	82.65 (12)
Cu1–N4	1.929 (3)	N1–Pd1–O6	167.36 (12)
Cu1–O3	1.975 (3)	O1–Pd1–O6	109.51 (11)
Cu1–N5	2.003 (4)	N4–Cu1–O3	175.31 (13)
Cu1–N3	2.010 (4)	N4–Cu1–N5	82.49 (14)
Cu1–O2	2.268 (3)	O3–Cu1–N5	98.60 (13)
Cu2–N7	1.928 (3)	N4–Cu1–N3	82.14 (14)
Cu2–O5	1.977 (3)	O3–Cu1–N3	96.56 (13)
Cu2–N8	1.995 (3)	N5–Cu1–N3	164.49 (14)
Cu2–N6	2.015 (3)	N4–Cu1–O2	104.60 (13)
Cu2–O4	2.367 (3)	O3–Cu1–O2	79.81 (11)
Cu2–O8^{i}	2.622 (3)	N5–Cu1–O2	98.10 (14)
		N3–Cu1–O2	87.77 (13)
		N7–Cu2–O5	178.46 (13)
		N7–Cu2–N8	82.60 (13)
		O5–Cu2–N8	98.69 (12)
		N7–Cu2–N6	82.01 (13)
		O5–Cu2–N6	96.76 (12)
		N8–Cu2–N6	163.99 (13)
		N7–Cu2–O4	101.11 (12)
		O5–Cu2–O4	77.91 (10)
		N8–Cu2–O4	97.32 (12)
		N6–Cu2–O4	89.97 (12)
		N7–Cu2–O8^{i}	98.69 (12)
		O5–Cu2–O8^{i}	82.04 (10)
		N8–Cu2–O8^{i}	96.01 (12)
		N6–Cu2–O8^{i}	81.98 (12)
		O4–Cu2–O8^{i}	157.35 (10)

[a]Symmetry code: (i) = x, $-y + 1/2$, $z + 1/2$.

powder X-ray diffraction patterns assures that the polycrystalline samples used in the magnetic measurements and the single crystals have the same crystal structure.

Magnetic Properties. The magnetic properties on polycrystalline samples of the complexes **3**–**5** were investigated in the temperature range of 2.0–300 K. Since the magnetic data of **5** were found to be practically identical to those of **4**, we will focus herein on the magnetic properties of **3** and **4**.

The temperature dependence of the $\chi_M T$ for **3** [χ_M is the magnetic susceptibility per four copper(II) ions, and T is the temperature] is shown in Figure S15 of the Supporting Information. At room temperature, $\chi_M T$ is equal to 1.60 cm^3 mol^{-1} K, in agreement with the value expected for four magnetically noninteracting paramagnetic copper(II) ions [$\chi_M T$ = 1.65 cm^3 mol^{-1} K with S_{Cu} = 1/2 and g_{Cu}= 2.10]. Upon cooling, $\chi_M T$ remains constant until about 10 K, and it further decreases slightly to 1.40 cm^3 mol^{-1} K at 2.0 K. This plot is typical of a very weak antiferromagnetic coupling between the copper(II) ions.

Apart from the possible intermolecular magnetic interactions, two intramolecular exchange pathways could be responsible for this weak magnetic coupling: (i) the one through the bis(oxamate)palladate(II) concerning the Cu1–Pd1–Cu4 and Cu2–Pd2–Cu3 trinuclear units and (ii) the other one across the phenylene rings involving Cu1 and Cu2 (O2–C2–N1–C3–C4–C5–N2–C9–O4) and Cu3 and Cu4 (O9–C12–N3–C13–C14–C15–N4–C19–O10). On the basis of previous magneto-structural studies where weak magnetic interactions between first-row transition metal ions were mediated by diamagnetic ions,[35,57–61] we assume that most likely, the presence of the HOMOs of the bis(oxamate)-palladate(II) bridging motif would be responsible for the transmission of the electronic interaction [exchange pathway (i)].

Consequently, we analyzed the magnetic data of **3** through the spin Hamiltonian of eq 1, the expression for the magnetic susceptibility being given by eq 2:

$$H = -J_{Cu1Cu4} S_{Cu1} S_{Cu4} - J_{Cu2Cu3} S_{Cu2} S_{Cu3} + \beta H(g_{Cu1} S_{Cu1} + g_{Cu2} S_{Cu2} + g_{Cu3} S_{Cu3} + g_{Cu4} S_{Cu4}) \quad (1)$$

$$\chi_M = (4N\beta^2 g^2/kT)[3 + \exp(-J/kT)]^{-1} \quad (2)$$

where $J = J_{Cu1Cu4} = J_{Cu2Cu3}$, $g = g_{Cu1} = g_{Cu2} = g_{Cu3} = g_{Cu4}$, and N, β, and k have their usual meanings. Least-squares best-fit parameters for **3** are J = −0.79(3) cm^{-1}; g = 2.08(1); and R = 4.5 × 10^{-5} {R is the agreement factor defined as $\Sigma[(\chi_M T)_{calcd} - (\chi_M T)_{obsd}]^2]\}/\ \Sigma[(\chi_M T)_{obsd}]^2\}$. This very weak antiferromagnetic coupling between the copper(II) ions mediated by the diamagnetic bis-bidentate [Pd(opba)]$^{2-}$ ligand in **3** [copper(II)–copper(II) separation about 10.8 Å] would correspond to the upper limit given that we have neglected any intermolecular antiferromagnetic interaction (the shortest intermolecular copper–copper distance being about 8.0 Å).

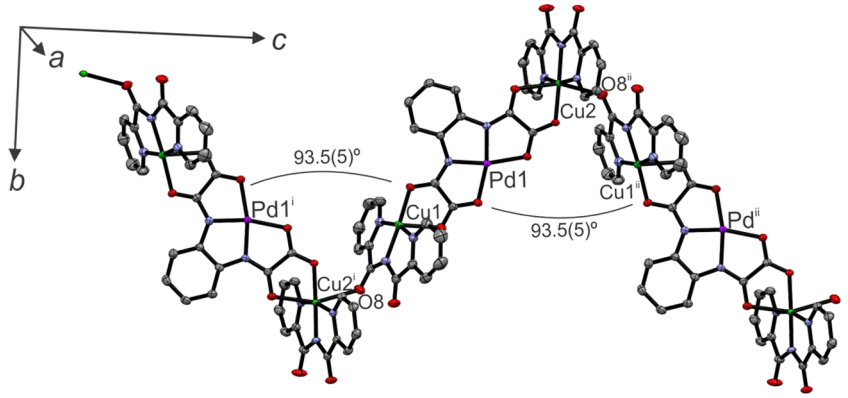

Figure 7. View of a fragment of the zigzag chain of trinuclear units growing along the crystallographic c-axis. Solvent molecules and hydrogen atoms are omitted for clarity [symmetry code: (i) = x, $1/2 - y$, $-1/2 + z$; (ii) = x, $1/2 - y$, $1/2 + z$].

DOI: 10.1021/cg5017388
Cryst. Growth Des. 2015, 15, 1325–1335

The magnetic properties of compound **4** in the form of the $\chi_M T$ versus T plot are shown in Figure S16 of the Supporting Information. They are very similar to those observed for **3**. At room temperature, the $\chi_M T$ is equal to 0.77 $cm^3\ mol^{-1}$ K, a value that is close to the expected for two copper(II) ions magnetically isolated. Upon cooling, this value remains constant until about 50.3 K, and then it slightly decreases to 0.65 $cm^3\ mol^{-1}$ K at 2.6 K. This is characteristic of a very weak antiferromagnetic interaction between spin doublets.

The crystal structure of **4** shows the presence of two possible exchange pathways: (i) the diamagnetic bis-bidentate $[Pd(opba)]^{2-}$ unit within the heterobimetallic Cu1−Pd1−Cu2 trinuclear entity (Cu1···Cu2 ca. 10.5 Å), which was shown to be involved in **3**, and (ii) the intertrimer double out-of-plane copper(II) to carbonyl(bpca)-oxygen skeleton (Cu1···$Cu2^i$ ca. 5.2 Å; see Figure 5). Given that the unpaired electron at each copper(II) ion in **4** is essentially located in the basal plane, the spin density predicted on the axial sites occupied by O7 at $Cu2^i$ [$Cu2^i$−O7 = 2.877(6) Å] and O9 at Cu1 [Cu1−$O9^i$ = 3.095(6) Å] would be extremely weak and then, the (ii) pathway is in principle to be ruled out.

Consequently, the magnetic data of **4** were analyzed through a simple Bleaney−Bowers expression for two spin doublets [eq 3]:

$$\chi_M = (2N\beta^2 g^2/kT)[3 + \exp(-J/kT)]^{-1} \quad (3)$$

where J is the magnetic coupling between Cu1 and Cu2 within the Cu1−Pd1−Cu2 trinuclear unit, and g is the average Landé factor ($g = g_{Cu1} = g_{Cu2}$). Least-squares best-fit parameters are J = −0.88(1) cm^{-1}, g = 2.03(1), and $R = 3.0 \times 10^{-5}$. The magnetic coupling in **4** is practically the same as that obtained for **3**, a feature that validates our assumption concerning the trinuclear Cu^{II}−Pd^{II}−Cu^{II} model as responsible for the magnetic coupling observed in **3** and **4**. Additional support to this conclusion is provided by the fact that the magnetic properties of **5** are practically identical to those of **4**. In this respect, one can see in Figure 7 that the trinuclear Cu1−Pd1−Cu2 entities (Cu1···Cu2 ca. 10.7 Å) are interlinked by single axial copper(II) to carbonyl(bpca)-oxygen interactions [Cu2−$O8^{ii}$ = 2.622(3) Å with Cu2···$Cu1^{ii}$ ca. 5.7 Å], the weak magnetic coupling in **5** being then mediated by the diamagnetic bis(oxamate)palladate-(II) unit.

CONCLUSIONS

In summary, we have described the synthesis, structural characterization, and magnetic properties of palladium(II)−copper(II) complexes as a result of the self-assembly process: one hexanuclear $Pd^{II}_2Cu^{II}_4$ compound (**3**), and two chains with linear (**4**) and zigzag (**5**) topologies with the same crystalline asymmetric unit Cu^{II}−Pd^{II}−Cu^{II}. Two dipalladium(II) building blocks have also been described, $K_4[Pd_2(mpba)_2] \cdot 4H_2O$ (**1**) and $K_4[Pd_2(mpba)_2] \cdot H_2O \cdot$ dmso (**2**), but only the crystal structure of **2** was determined by X-ray diffraction. It was shown that **2** exhibits a 3D coordination network in which the potassium(I) ions are responsible to connect the anionic units. Compound **3** presents a hexanuclear structure made up of two trinuclear Cu^{II}−Pd^{II}−Cu^{II} units connected via mpba ligands. It is worth noting that compounds **4** and **5** have the same trinuclear Cu^{II}−Pd^{II}−Cu^{II} core but with a different interlinking. Both **4** and **5** form neutral chains but linear for **4** and zigzag for **5**. The difference in the molecular architecture can be understood in the light of the synthesis process considering that compound **5** is obtained by cooling very slowly the mother liquor compared to what is done for **4**. As a matter of fact, this paper illustrates an example of the importance of the control of the parameters in the synthesis concerning the crystal engineering of oxamate-containing complexes. The magnetic properties in **3** and **4** correspond to weak antiferromagnetic interactions between the paramagnetic $[Cu(bpca)]^+$ units through the diamagnetic bis(oxamate)palladate(II) pathway [J_{CuPdCu} = −0.79(3) (**3**) and −0.88(1) cm^{-1} (**4**)]. To the best of our knowledge, it is the first time that this kind of coordination mode in **5** has been obtained for [bis(2-pyridylcarbonyl)amidate]copper(II) complexes.

ASSOCIATED CONTENT

Supporting Information

X-ray powder diffraction patterns for **2**−**5**, IR data and thermal analyses measurements for all compounds. This material is available free of charge via the Internet at http://pubs.acs.org.

AUTHOR INFORMATION

Corresponding Author

*E-mail: cynthialopes@ufmg.br.

Notes

The authors declare no competing financial interest.

ACKNOWLEDGMENTS

The authors thank the Conselho Nacional de Desenvolvimento Científico e Tecnológico (CNPq), the Fundação de Amparo à Pesquisa do Estado de Minas Gerais (FAPEMIG), the Coordenação de Aperfeiçoamento de Pessoal de Nível Superior (CAPES), and the Ministerio Español de Economía y Competitividad (Projects CTQ2013-44844P and HB2012-0290) for financial support.

REFERENCES

(1) Kumar, G.; Gupta, R. *Chem. Soc. Rev.* **2013**, *42*, 9403−9453.
(2) Whitesides, G. M.; Grzybowski, B. *Science* **2002**, *295*, 2418−2421.
(3) Zheng, Y.-Z.; Zhou, G.-J.; Zhengab, Z.; Winpenny, R. E. P. *Chem. Soc. Rev.* **2014**, *43*, 1462−1475.
(4) Coronado, E.; Day, P. *Chem. Rev.* **2004**, *104*, 5419−5448.
(5) Alivisatos, A. P.; Barbara, P. F.; Castleman, A. W.; Chang, J.; Dixon, D. A.; Klein, M. L.; McLendon, G. L.; Miller, J. S.; Ratner, M. A.; Rossky, P. J.; Stupp, S. I.; Thompson, M. E. *Adv. Mater.* **1998**, *10*, 1297−1336.
(6) Verdaguer, M.; Bleuzen, A.; Marvaud, V.; Vaissermann, J.; Seuleiman, M.; Desplanches, C.; Scuiller, A.; Train, C.; Garde, R.; Gelly, G.; Lomenech, C.; Rosenman, I.; Veillet, P.; Cartier, C.; Villain, F. *Coord. Chem. Rev.* **1999**, *190*−*192*, 1023−1047.
(7) Lescouëzec, R.; Toma, L. M.; Vaissermann, J.; Verdaguer, M.; Delgado, F. S.; Ruiz-Pérez, C.; Lloret, F.; Julve, M. *Coord. Chem. Rev.* **2005**, *249*, 2691−2729.
(8) Wang, S.; Ding, X.-H.; Li, Y.-H.; Huang, W. *Coord. Chem. Rev.* **2012**, *256*, 439−464.
(9) Marinescu, G.; Andruh, M.; Lloret, F.; Julve, M. *Coord. Chem. Rev.* **2011**, *255*, 161−185.
(10) Fortea-Pérez, F. R.; Vallejo, J.; Inclán, M.; Déniz, M.; Pasán, J.; García-España, E.; Julve, M. *J. Coord. Chem.* **2013**, *66*, 3349−3364.
(11) Decurtins, S.; Pelleaux, R.; Antorena, G.; Palacio, F. *Coord. Chem. Rev.* **1999**, *190*−*192*, 841−854.
(12) Pilkington, M.; Decurtins, S. *Magnetism: Molecules to Materials II*; Miller, J. S., Drillon, M., Eds; Wiley-VCH, Verlag: Weinheim, Germany, 2001; p 339.
(13) Gruselle, M.; Train, C.; Boubekeur, K.; Gredin, P.; Ovanesyan, N. *Coord. Chem. Rev.* **2006**, *250*, 2491−2500.

DOI: 10.1021/cg5017388
Cryst. Growth Des. 2015, 15, 1325−1335

(14) Pilkington, M.; Decurtins, S. *Comprehensive Coordination Chemistry: II. From Biolgy to Nanotechnology*; MacCleverthy, J. A., Meyer, T. J., Eds; Elsevier: Amsterdam, 2007; Vol. 7, p 177.
(15) Train, C.; Gheorghe, R.; Krstic, V.; Chamoreau, L. M.; Ovanesyan, N. S.; Rikken, G. L. J. A.; Gruselle, M.; Verdaguer, M. *Nat. Mater.* **2008**, *7*, 729−734.
(16) Okawa, H.; Shigematsu, A.; Sadakiyo, M.; Miyagawa, T.; Noyeda, K.; Ohba, M.; Kitagawa, H. *J. Am. Chem. Soc.* **2009**, *131*, 13516−13522.
(17) Clemente-León, M.; Coronado, E.; Martí-Gastaldo, C.; Romero, F. M. *Chem. Soc. Rev.* **2011**, *40*, 473−497.
(18) Pardo, E.; Train, C.; Liu, H.; Chamoreau, L. M.; Dhkil, B.; Boubekeur, K.; Lloret, F.; Nakatani, K.; Tokoro, H.; Ohkoshi, S.-I.; Verdaguer, M. *Angew. Chem., Int. Ed.* **2012**, *51*, 8356−8360.
(19) Okawa, H.; Sadakiyo, M.; Yamada, T.; Ohba, M.; Kitagawa, H. *J. Am. Chem. Soc.* **2013**, *135*, 2256−2262.
(20) Maxim, C.; Ferlay, S.; Tokoro, H.; Ohkoshi, S.-I.; Train, C. *Chem. Commun.* **2014**, *50*, 5629−5632.
(21) Ruiz, R.; Faus, J.; Lloret, F.; Julve, M.; Journaux, Y. *Coord. Chem. Rev.* **1999**, *193*−*195*, 1069−1117.
(22) Pardo, E.; Ruiz-García, R.; Cano, J.; Ottenwaelder, X.; Lescouëzec, R.; Journaux, Y.; Lloret, F.; Julve, M. *Dalton Trans.* **2008**, 2780−2805.
(23) Dul, M. C.; Pardo, E.; Lescouëzec, R.; Journaux, Y.; Ferrando-Soria, J.; Ruiz-García, R.; Cano, J.; Julve, M.; Lloret, F.; Cangussu, D.; Pereira, C. L. M.; Stumpf, H. O.; Pasán, J.; Ruiz-Pérez, C. *Coord. Chem. Rev.* **2010**, *254*, 2281−2296.
(24) Grancha, T.; Ferrando-Soria, J.; Castellano, M.; Julve, M.; Pasán, J.; Armentano, D.; Pardo, E. *Chem. Commun.* **2014**, *50*, 7569−7585.
(25) Pereira, C. L. M.; Pedroso, E. F.; Doriguetto, A. C.; Ellena, J. A.; Boubekeur, K.; Filali, Y.; Journaux, Y.; Novak, M. A.; Stumpf, H. O. *Dalton Trans.* **2011**, *40*, 746−754.
(26) do Pim, W. D.; Oliveira, W. X. C.; Ribeiro, M. A.; de Faria, E. N.; Teixeira, I. F.; Stumpf, H. O.; Lago, R. M.; Pereira, C. L. M.; Pinheiro, C. B.; Figueiredo-Júnior, J. C. D.; Nunes, W. C.; de Souza, P. P.; Pedroso, E. F.; Castellano, M.; Cano, J.; Julve, M. *Chem. Commun.* **2013**, *49*, 10778−10780.
(27) Pardo, E.; Ruiz-García, R.; Lloret, F.; Faus, J.; Julve, M.; Journaux, Y.; Delgado, F.; Ruiz-Pérez, C. *Adv. Mater.* **2004**, *16*, 1597−1600.
(28) Fortea-Pérez, F. R.; Vallejo, J.; Julve, M.; Lloret, F.; De Munno, G.; Armentano, D.; Pardo, E. *Inorg. Chem.* **2013**, *52*, 4777−4779.
(29) Vallejo, J.; Pascual-Alvarez, A.; Cano, J.; Castro, I.; Julve, M.; Lloret, F.; Krzystek, J.; De Munno, G.; Armentano, D.; Wernsdorfer, W.; Ruiz-García, R.; Pardo, E. *Angew. Chem., Int. Ed.* **2014**, *52*, 14075−14079.
(30) Oliveira, W. X. C.; da Costa, M. M.; Fontes, A. P. S.; Pinheiro, C. B.; de Paula, F. C. S.; Jaimes, E. H. L.; Pedroso, E. F.; de Souza, P. P.; Pereira-Maia, E. C.; Pereira, C. L. M. *Polyhedron* **2014**, *76*, 16−21.
(31) Fortea-Pérez, F. R.; Schlegel, I.; Julve, M.; Armentano, D.; De Munno, G.; Stiriba, S. E. *J. Organomet. Chem.* **2013**, *743*, 102−108.
(32) Fortea-Pérez, F. R.; Marino, N.; Armentano, D.; De Munno, G.; Julve, M.; Stiriba, S. E. *CrystEngComm* **2014**, *16*, 6971−6988.
(33) Fortea-Pérez, F. R.; Armentano, D.; Julve, M.; De Munno, G.; Stiriba, S. E. *J. Coord. Chem.* **2014**, *67*, 4003−4015.
(34) Simões, T. R. G.; Mambrini, R. V.; Reis, D. O.; Marinho, M. V.; Ribeiro, M. A.; Pinheiro, C. B.; Ferrando-Soria, J.; Déniz, M.; Ruiz-Pérez, C.; Cangussu, D.; Stumpf, H. O.; Lloret, F.; Julve, M. *Dalton Trans.* **2013**, *42*, 5778−5795.
(35) Oliveira, W. X. C.; Ribeiro, M. A.; Pinheiro, C. B.; Nunes, W. C.; Julve, M.; Journaux, Y.; Stumpf, H. O.; Pereira, C. L. M. *Eur. J. Inorg. Chem.* **2012**, *34*, 5685−5693.
(36) Castro, I.; Faus, J.; Julve, M.; Amigó, J. M.; Sletten, J.; Debaerdemaeker, T. *J. Chem. Soc., Dalton Trans.* **1990**, 891−897.
(37) Fernández, I.; Ruiz, R.; Faus, J.; Julve, M.; Lloret, F.; Cano, J.; Ottenwaelder, X.; Journaux, Y.; Muñoz, M. C. *Angew. Chem., Int. Ed.* **2001**, *40*, 3039−3042.
(38) Earnshaw, A. *Introduction to Magnetochemistry*; Academic Press: London, 1968.
(39) Xcalibur CCD system. *CrysAlisPro Software System, version 1.171.35.15*; Agilent Technologies UK Ltd: Oxford, 2011.
(40) Sheldrick, G. M. *Acta Crystallogr.* **2008**, *A64*, 112−122.
(41) Palatinusz, L.; Chapuis, G. *J. Appl. Crystallogr.* **2007**, *40*, 786−790.
(42) Sheldrick, G. M. *SHELXL-97 Program for Crystal Structure Refinement*; University of Göttingen: Germany, 1997.
(43) Johnson, C. K. In *Crystallographic Computing*; Ahmed, F. R., Ed.; Munksgaard: Copenhagen, 1970; pp 207−219.
(44) Caires, F. J.; Lima, L. S.; Carvalho, C. T.; Siqueira, A. B.; Treu-Filho, O.; Ionashiro, M. *J. Therm. Anal. Calorim.* **2012**, *107*, 335−344.
(45) Ma, J. C.; Dougherty, D. A. *Chem. Rev.* **1997**, *97*, 1303−1324.
(46) Reyes-Martínez, R.; Höpfl, H.; Godoy-Alcántar, C.; Medrano, F.; Tlahuext, H. *CrystEngComm* **2009**, *11*, 2417−2424.
(47) Martin, T. W.; Derewenda, Z. S. *Nat. Struct. Biol.* **1999**, *6*, 403−406.
(48) Addison, A. W.; Rao, T. N.; Reedijk, J.; Van Rijn, J.; Verschoor, G. C. *J. Chem. Soc., Dalton Trans.* **1984**, 1349−1356.
(49) Lerner, E. I.; Lippard, S. J. *J. Am. Chem. Soc.* **1976**, *98*, 5397−5398.
(50) Lerner, E. I.; Lippard, S. J. *Inorg. Chem.* **1977**, *16*, 1546−1551.
(51) Folgado, J. V.; Coronado, E.; Beltrán-Porter, D.; Burriel, R.; Fuertes, A.; Miratvilles, C. *J. Chem. Soc., Dalton Trans.* **1988**, 3041−3046.
(52) Castro, I.; Faus, J.; Julve, M.; Journaux, Y.; Sletten, J. *J. Chem. Soc., Dalton Trans.* **1991**, 2533−2538.
(53) Halder, P.; Zangrando, E.; Paine, T. K. *Polyhedron* **2010**, *29*, 434−440.
(54) Casellas, H.; Costantino, F.; Mandonnet, A.; Caneschi, A.; Gatteschi, D. *Inorg. Chim. Acta* **2005**, *358*, 177−185.
(55) Carlucci, L.; Ciani, G.; Maggini, S.; Proserpio, D. M.; Sessoli, R.; Totti, F. *Inorg. Chim. Acta* **2011**, *376*, 538−548.
(56) Xu, W.; Pan, W.-J.; Zheng, Y.-Q. *J. Coord. Chem.* **2013**, *66*, 4415−4429.
(57) Journaux, Y.; Sletten, J.; Kahn, O. *Inorg. Chem.* **1986**, *25*, 439−447.
(58) Lloret, F.; Journaux, Y.; Julve, M. *Inorg. Chem.* **1990**, *36*, 3967−3972.
(59) Chaudhuri, P.; Winter, M.; Védova, B. P. C. D.; Bill, E.; Trautwein, A.; Gehring, S.; Fleischhauer, P.; Nuber, B.; Weiss, J. *Inorg. Chem.* **1991**, *30*, 2148−2157.
(60) Ruiz, R.; Julve, M.; Faus, J.; Lloret, F.; Muñoz, M. C.; Journaux, Y.; Bois, C. *Inorg. Chem.* **1997**, *36*, 3434−3439.
(61) Buvaylo, E. A.; Kokozay, V. N.; Vassilyeva, O. Y.; Skelton, B. W.; Jezierska, J.; Brunel, L. C.; Ozarowski, A. *Chem. Commun.* **2005**, 4976−4978.

DOI: 10.1021/cg5017388
Cryst. Growth Des. 2015, 15, 1325−1335